Computer Assisted Mechanics and Engineering Sciences, 13: 613–625, 2006.

Modelling of freezing in frost-susceptible soils

Radosław L. Michałowski
Department of Civil and Environmental Engineering, University of Michigan
Ann Arbor, MI 48109, U.S.A.

Ming Zhu
GeoSyntec Consultants, Kennesaw, GA 30144, U.S.A.
(formerly graduate student at University of Michigan)

(Received in the final form November 15, 2006)

Frost heave in soils is a common phenomenon in cold regions, yet the previous efforts toward its mathematical description did not result into a generally accepted model. The model described in this paper is based on the concept of porosity rate function, which characterizes well the heaving phenomenon in variety of soils. The concept is simple enough so that it can be easily incorporated in numerical methods. The description of the model is followed by brief considerations of energy transfer and phase change. Calibration results are shown, and the model is implemented to solve a practical boundary value problem. The influence of thermal insulation on the performance of a retaining wall with frost-susceptible backfill is discussed.

Keywords: soil freezing, frost heave, constitutive model, heat transfer, phase change, retaining wall

1. INTRODUCTION

Frost heaving and thawing contributes to significant damage of transportation infrastructure every freezing season. First systematic research focused on frost heaving of soils was published by Taber [19, 20], and Beskow [1]. However, intensive efforts to rigorously describe the process of soil freezing and the related frost heave did not start until the 1980's. These efforts were preceded by the capillary theory of frost heaving, based on the Laplace surface tension equation. While the simplicity of the capillary theory was appealing, the experimental tests did not confirm its validity: heaving pressures during freezing tests were found to be significantly larger than those predicted by the theory. There was also evidence that ice lenses can form within frozen soil at some distance from the freezing front, which could not be explained by the capillary theory.

The secondary frost heaving mechanism was proposed by Miller in 1978 [13]. This frost heave theory is based on a regelation mechanism, which causes the movement of particles embedded in ice subjected to a temperature gradient. A key experiment presenting the migration of particles in ice up the temperature gradient was shown by Römkens and Miller [16]. Pore ice and ice lenses are treated as one body in the secondary heave mechanism. Due to kinematical constraints, the mineral (solid) particles do not move up the temperature gradient, and thus it is the ice which moves down the temperature gradient, the relative particle-ice motion being the same. This mechanism gives rise to secondary frost heave, and its mathematical description is often called the *rigid ice model.* Attempts at practical calculations of frost heave using the rigid ice model can be found in papers by O'Neil and Miller [14, 15], Holden [6], and Holden *et al.* [7].

The *rigid ice model* received the most attention in the literature, though other useful models can be found (e.g., Konrad and Morgenstern [8], Guymon *et al.* [5], Shen and Ladanyi [18]). A common characteristic of the aforementioned models is that they consider the process of freezing at the

microscopic level (i.e., they consider formation of a single ice lens). The Clausius-Clapeyron equation is utilized to relate pressure to temperature at the water-ice interface. Little attention has been paid to constitutive modelling of soils, where frost susceptibility is defined as a property of the mineral-ice-water mixture. Such a macroscopic-level approach to modelling of frost susceptible soils was suggested by Blanchard and Frémond [2], and Michalowski [10, 11]. The same concept is used in this paper, though with a modified function representing the rate of porosity increase during freezing, in order to obtain a more realistic response of the soil to freezing. This model is described in more detail in a recent paper by Michalowski and Zhu [12], and here some aspects of application of this model to solving an engineering problem are shown.

As the macroscopic approach to modelling frost heave in soils is not widely accepted, the philosophy behind this approach is presented in the next section. The following section presents the porosity rate function and the unfrozen water content in frozen soil. Fundamental equations of the model are then presented in Sections 4 and 5, followed by calibration of the model, its validation, and simulation of freezing of a frost-susceptible backfill behind a retaining wall. The influence of thermal insulation on the performance of the retaining wall is also discussed.

2. Philosophy of approach

Of all frost heave models, it is the rigid ice model that received most attention. However, the current stage of development of this model allows only one-dimensional freezing simulations. Like the model based on capillary action, the secondary frost heave model is based on considering the micromechanical processes, and the heaving effect is obtained as an integral of the growth of all ice lenses in a frozen column (one-dimensional process). The term "micromechanical" here pertains to processes taking place among the constituents of the skeleton-ice-water mixture. Macromechanical (or global) effects are those seen as the response of the entire mixture (e.g., average porosity increase).

Constructing a model for predictions of frost heave based on the summation of the actual micromechanical processes will lead to realistic qualitative results. As to the quantitative results, the micromechanical approach may not necessarily be the most reliable one. This has certainly been true in the mechanics of solids, where phenomenological models based on introducing material parameters at the macroscopic level were far more successful than micromechanics-based models in predicting such global quantities as displacements or limit loads. The simplest examples of constitutive (of phenomenological) models are linear elasticity (Hook's model), and the model of perfect plasticity. As opposed to micromechanics-based models, they cannot explain why the deformation is elastic (or plastic), but they can be quite accurate in determining the magnitudes of strain or the stress state, given material properties defined at the macroscopic level (Young's modulus, Poisson's ratio, or the yield condition and the flow rule). Micromechanical models can explain the nature of the deformation, but the quantitative predictions are often orders of magnitude apart from the experimental results.

There is no reason to doubt that a phenomenological model formulated at the macroscopic level can be constructed for frost susceptible soils so that the increase of porosity due to ice lens formation can be modelled. While the material functions defined at the macroscopic level do not have to be derived from microscopic processes, their mathematical form must reflect the experimentally observed effects. For a frost susceptible soil model this effect is the increase in volume which will be modelled by a *porosity rate function*, $\dot{n}$, as suggested earlier (Frémond [3] and Michalowski [10, 11]). Thus the ice growth will be described as the average increase in porosity (or volume) of the soil element, rather than as separate ice lenses growth.

The frost heave itself is a process which occurs when the frost susceptible soil is placed under certain conditions. Thus, frost heave can be calculated as the solution to a boundary value problem in which the soil is subjected to specific initial and thermal boundary conditions. While frost susceptibility is a material property, frost heave is a process related to soil mass and specific boundary

conditions rather than to a soil element. In this sense, frost heave itself is not a property of the material, but frost susceptibility is.

To formulate and solve the problem of frost heave for specific thermal and hydraulic conditions, constitutive functions in addition to *porosity rate function* $\dot{n}$ need to be adopted: the unfrozen water content in frozen soil, the heat transfer and mass flow laws, and the rule describing deformation (and/or yielding) of the soil skeleton and the frozen composite. These equations, along with the fundamental principles of energy, mass, and momentum conservation, form the set of equations to be solved for given initial and boundary conditions.

Related to the approach proposed is the interpretation of the freezing soil as a *heat engine*. Heaving soil performs mechanical work against external loads (gravity and boundary forces), and also performs work which is either dissipated (e.g., during irreversible deformation of the mixture) or stored as elastic energy (in the mineral skeleton). Thus it can be argued that part of the latent heat released when water freezes is transformed into mechanical work by means of a heat engine of a very low efficiency. While the temperature gradients at the macroscopic level are considered finite within the freezing soil, the specific conditions for the heat engine (thermal discontinuity) must exist at the microscopic level.

As all functions are formulated at the macroscopic level, this approach does not utilize the Clausius-Clapeyron equation which is used in the micromechanics-based approach (analysis of a single ice lens formation).

3. Fundamental functions

The formation of a single ice lens is not considered here; rather, the ice growth is modelled as an increase in porosity in a finite volume of the soil. Consequently, the fundamental function that describes the ice growth is selected in a form of a porosity rate relation. This function captures the fundamental features of the process; it describes an intense growth of porosity at temperatures slightly below freezing, and decaying growth with the further drop in the temperature. The core of the porosity rate function, $\dot{n}$, has been selected in the following form,

$$\dot{n} = \dot{n}_m \left(\frac{T - T_0}{T_m} \right)^2 \exp \left[1 - \left(\frac{T - T_0}{T_m} \right)^2 \right] \tag{1}$$

where $\dot{n}_m$ is the maximum porosity rate, and T_m is the temperature at which this maximum occurs; T_0 is the freezing point of water. This function has all the necessary characteristics of a heaving soil, and its graphical representation is shown in Fig. 1.

The function with the higher peak (Fig. 1) is typical of silts, which heave very intensely at a temperature slightly below freezing, but quickly taper off as the temperature drops down. Clays, on the other hand, can heave at lower temperatures, but the intensity of heaving is not as high (the dashed line in Fig. 1).

The function in Eq. (1) is not sensitive to the temperature gradient, and is not affected by the stress state. Therefore, two multipliers are now included with this function to account for both the temperature gradient and the stress state,

$$\dot{n} = \dot{n}_m \left(\frac{T - T_0}{T_m} \right)^2 \exp \left[1 - \left(\frac{T - T_0}{T_m} \right)^2 \right] \frac{\left| \frac{\partial T}{\partial l} \right|}{g_T} \exp \left(- \frac{|\bar{\sigma}_{kk}|}{\varsigma} \right). \tag{2}$$

The quotient $\left| \frac{\partial T}{\partial l} \right| / g_T$ represents linear dependency of the porosity rate on the temperature gradient in the direction of the heat flow (direction l). g_T is a temperature gradient at which $\dot{n}_m$ is evaluated ($\dot{n}_m / g_T$ is a constant material property for a given soil). The last factor in Eq. (2) includes the influence of the stress state on frost heave. Experimental data on the influence of the stress state on frost heave are scarce. However, it is intuitively understood that the retardation of frost heave is caused predominantly by the normal stress in the direction of heat flow within the freezing

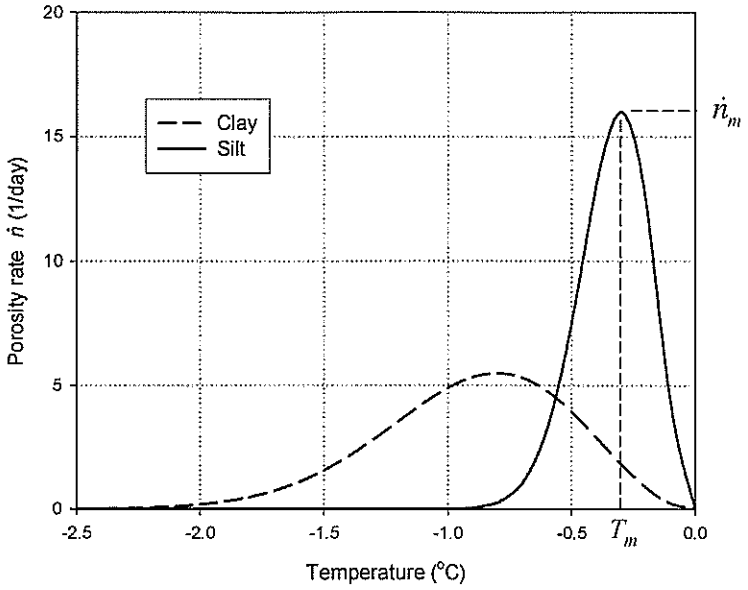

Fig. 1. Porosity rate function for clay and silt

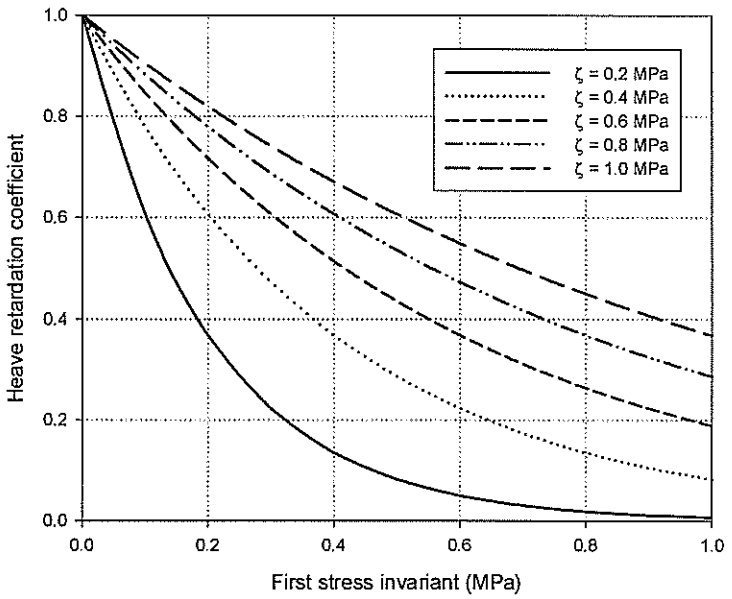

Fig. 2. The influence of the stress state on the porosity rate in freezing soils

zone (frozen fringe), with some contribution of the normal stresses in the other two perpendicular directions. Consequently, it was decided to choose a function of the first invariant of the Cauchy stress tensor. This retardation coefficient is graphically represented in Fig. 2.

The second constitutive function important in modelling of freezing of soils is the unfrozen water content in frozen soil. When the freezing front moves into soils such as clay or silt, not all water changes phase. While the amount of unfrozen water drops down with the decrease in temperature, its presence plays an important role in the energy balance as the latent heat is released from freezing soil even at temperatures well below freezing point of water. The function adopted for describing the unfrozen water content is given as

$$w = w^* + (\bar{w} - w^*)\, e^{a(T-T_0)} \tag{3}$$

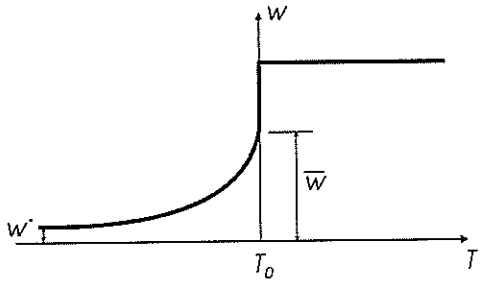

Fig. 3. Unfrozen water content in frozen soil

and it is presented graphically in Fig. 3. Not all water in soil freezes at the freezing point of water T_0; rather there is a discontinuity at T_0, and the liquid water content drops down to some amount of $\bar{w}$, and it then decays to a small content of w^* at some reference low temperature. This relation is graphically represented in Fig. 3.

The functions in Eqs. (2) and (3) are the fundamental functions for simulating freezing in frost susceptible soils.

4. Porosity growth tensor

The porosity rate function in Eq. (2) yields a scalar quantity. However, during freezing the soil does not grow in an isotropic manner. In fact, there is ample experimental evidence that ice lenses grow predominantly in the direction of heat flow lines. Therefore, the porosity rate needs to be given a tensorial character.

We introduce here a unit growth tensor (see [11]) defined as

$$\alpha_{ij} = \begin{vmatrix} \alpha_{11} & \alpha_{12} & \alpha_{13} \\ \alpha_{21} & \alpha_{22} & \alpha_{23} \\ \alpha_{31} & \alpha_{32} & \alpha_{33} \end{vmatrix} = \begin{vmatrix} \xi & 0 & 0 \\ 0 & (1-\xi)/2 & 0 \\ 0 & 0 & (1-\xi)/2 \end{vmatrix}. \tag{4}$$

The principal direction ℓ of the unit growth tensor α_{ij} (associated with the major growth) coincides with the heat flow lines.

Coefficient ξ indicates the directional characteristic of the growth; it can vary in the range of 0.33 to 1. The porosity growth tensor is then defined as

$$\dot{n}_{ij} = \dot{n}\alpha_{ij} \tag{5}$$

where $\dot{n}_{ij}$ is a tensor that is analogous to the strain rate tensor, and it can be included directly in the continuum model of the freezing soil. When $\xi = 1$, the growth occurs unidirectionally, whereas the growth becomes isotropic when $\xi = 0.33$. Different "patterns" of anisotropic growth can be modelled by assuming ξ anywhere between 0.33 and 1.

The porosity growth tensor can be used directly to determine the strain increments, provided the account is taken for associated deformation of the soil. One-dimensional simulation was used first to calibrate the model and then, in order to validate the model, a process with different initial/boundary conditions was predicted and compared to experimental results. In one-dimensional process, the relation of the porosity increase and the non-zero normal strain increment in elastic continuum is

$$\mathrm{d}\varepsilon_l = \frac{\mu + \xi(1-2\mu)}{1-\mu}\,\dot{n}\,\mathrm{d}t \tag{6}$$

where μ is the Poisson's ratio. Hence, only when the porosity growth is one-dimensional, $\xi = 1$, does the entire growth translate into the strain increment. If the soil is elastic and plain strain is considered, the increments of strain due to growth of porosity appear to be

$$\left\{ \begin{array}{c} \mathrm{d}\varepsilon_{11} \\ \mathrm{d}\varepsilon_{22} \\ \mathrm{d}\gamma_{12} \end{array} \right\} = \left\{ \begin{array}{c} \xi + \mu(1-\xi)/2 \\ (1+\mu)(1-\xi)/2 \\ 0 \end{array} \right\} \dot{n}\,\mathrm{d}t. \tag{7}$$

5. Balance equations

For convenience, we introduce the unfrozen water concentration ν in frozen soil (volumetric fraction)

$$\nu = \frac{V^{\mathrm{w}}}{V^{\mathrm{i}} + V^{\mathrm{w}}} \tag{8}$$

where V^{w} and V^{i} are volumes of water and ice, respectively. The volumetric fractions of the frozen composite are then expressed as

$$\begin{aligned} \theta^{\mathrm{s}} &= \frac{V^{\mathrm{s}}}{V} = 1 - n, \\ \theta^{\mathrm{w}} &= \frac{V^{\mathrm{w}}}{V} = \nu n, \\ \theta^{\mathrm{i}} &= \frac{V^{\mathrm{i}}}{V} = n(1-\nu) \end{aligned} \tag{9}$$

where n is the porosity (ratio of the pore volume to the volume of the mixture), and superscripts s, w, and i denote the solid, water and ice fractions, respectively. Consequently, the average density ρ is

$$\rho = \theta^{\mathrm{s}}\rho^{\mathrm{s}} + \theta^{\mathrm{w}}\rho^{\mathrm{w}} + \theta^{\mathrm{i}}\rho^{\mathrm{i}} = (1-n)\rho^{\mathrm{s}} + \nu n\rho^{\mathrm{w}} + n(1-\nu)\rho^{\mathrm{i}} \tag{10}$$

and the specific heat capacity C (per unit volume) can be expressed as

$$C = (1-n)\rho^{\mathrm{s}}c^{\mathrm{s}} + \nu n\rho^{\mathrm{w}}c^{\mathrm{w}} + n(1-\nu)\rho^{\mathrm{i}}c^{\mathrm{i}} \tag{11}$$

where c^{s}, c^{w}, and c^{i} are the mass capacities of the mineral (solid), water, and ice, respectively.

Adopting now the Fourier heat conduction law, the energy balance becomes

$$C\frac{\partial T}{\partial t} - L\frac{\partial \theta^{\mathrm{i}}}{\partial t}\rho^{\mathrm{i}} - \nabla(\lambda\nabla T) = 0 \tag{12}$$

where the effective heat conductivity in the Fourier law was taken as

$$\lambda = \lambda_s^{\theta^{\mathrm{s}}}\lambda_w^{\theta^{\mathrm{w}}}\lambda_i^{\theta^{\mathrm{i}}}. \tag{13}$$

The mass balance, based on the Darcy law of the water transfer, takes the following form

$$(\rho^{\mathrm{i}} - \rho^{\mathrm{s}})\frac{\partial n}{\partial t} + (\rho^{\mathrm{w}} - \rho^{\mathrm{i}})\frac{\partial(n\nu)}{\partial t} - \rho^{\mathrm{w}}\nabla(k\nabla h) = 0 \tag{14}$$

where h is the hydraulic head, and k is the hydraulic conductivity in Darcy law.

6. Calibration

A set of experimental test results was identified to calibrate the model [4]. First the unfrozen water content was calibrated for the clay used in the experiments, and this calibration is shown in Fig. 4. This particular set of data was approximated with the function in Eq. (3), but without the discontinuity at the freezing point ($w^* = 5.8\%$, $\bar{w} = 28.5\%$, $a = 0.16$).

Nine tests with ramping boundary temperatures were given by Fukuda *et al.* [4], for variety of temperature gradients and different overburden pressure. A step freezing process was then simulated and compared to experimental results in order to validate the model.

The calibration process was performed by simulating the one-dimensional process using a column of 30 finite elements. The system ABAQUS was used to perform the calculations. Figure 5 illustrates the calibration process where the parameters of the model were selected such, so that the calculated frost heave matched the experimental results. The frost heaving curve indicates the increase of the specimen height during freezing with ramped temperatures at the cold and warm side of the specimen. The freezing front propagation associated with the ramping process appears to match the measured propagation well.

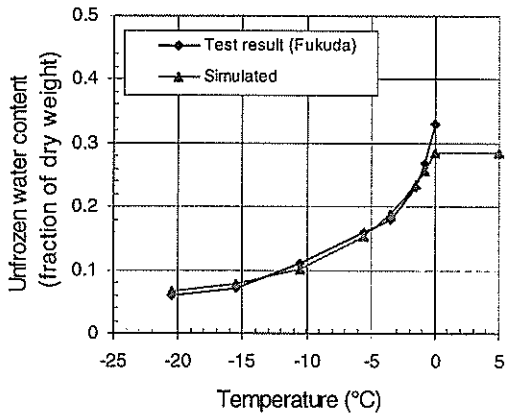

Fig. 4. Calibration of unfrozen water content in frozen soil (after [12])

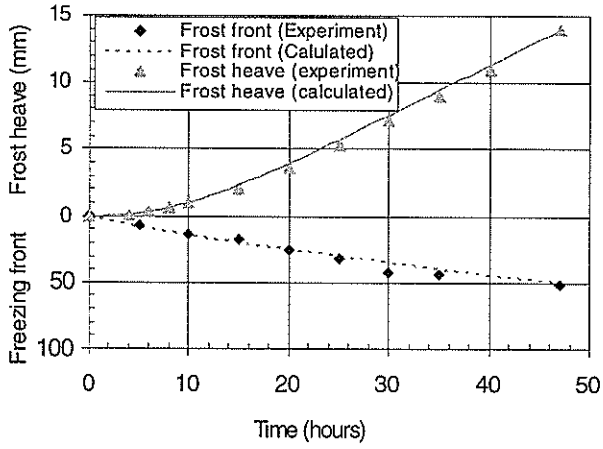

Fig. 5. Calibration of the model (after [12])

As the porosity rate model is a unique model with little application experience, it is of interest to indicate what are the reasonable values of the parameters in the porosity rate function in Eq. (2). For the clays tested by Fukuda *et al.* [4], the calibration process led to the following quantities: maximum porosity rate $\dot{n}_m = 6.02 \cdot 10^{-5}\,\mathrm{s}^{-1}$ (or $5.2 \cdot 1/24\,\mathrm{h}$) at $g_T = 100°\mathrm{C/m}$, or $\dot{n}_m/g_T = 6.02 \cdot 10^{-7}\,\mathrm{m°C^{-1}s^{-1}}$, $T_m = -0.87°\mathrm{C}$, and $\zeta = 0.6\,\mathrm{MPa}$.

7. Simulation of a step-freezing process

Once the model parameters for clay were evaluated, a step-freezing process was simulated. This step-freezing process was tested in a laboratory experiment by Fukuda *et al.* [4], and the results of this process were not used to calibrate the model. Cylindrical specimen size was 70 mm in height and 100 mm in diameter. The initial temperature of the specimen was uniform at 5°C, and, at time $t = 0$, the bottom plate temperature was dropped to −5°C and kept at −5°C for 115 hours.

The distribution of the increase in porosity is illustrated in Fig. 6. It is evident that once the freezing front moves through the soil quickly at the initial stage of the frost penetration, the in-situ freezing leaves an insignificant increase in porosity behind the freezing front. Once the freezing

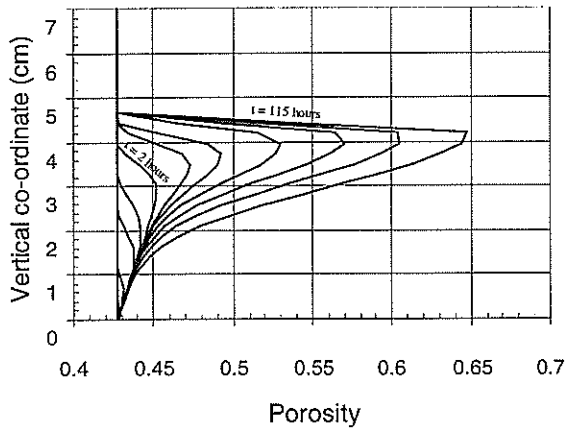

Fig. 6. Distribution of porosity during a step-freezing process

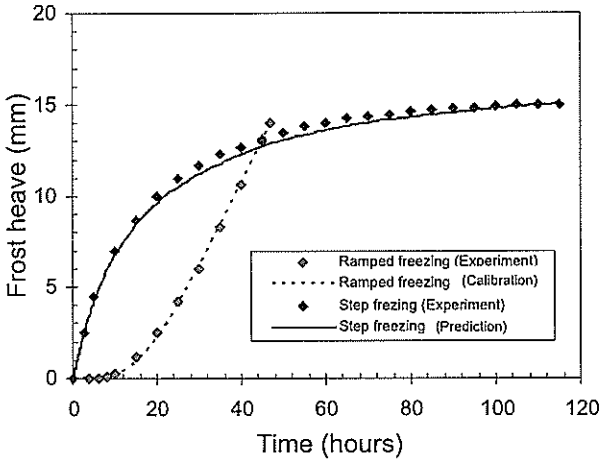

Fig. 7. Freezing processes: calibration and validation curves

front stabilizes at the level of about 4.5 cm in the specimen, the porosity increase becomes quite significant, indicative of ice lenses formation.

The predicted frost heave of the specimen is illustrated in Fig. 7 along with the calibration curve. The calibration frost heave process was the one with ramped temperatures, with the specimen subjected to freezing for 47 hours. The rate of frost heave is small at the beginning of the process, and it significantly increases after about 10 hours as a larger portion of the specimen starts contributing to the frost heave. The step freezing process used to validate the model has opposite characteristic: the rate of heave is large at the beginning, and it decays later in the process. The model prediction appears to coincide with the experimental measurements remarkably well.

8. Application of the Model – Freezing of Frost-Susceptible Backfill Behind a Retaining Wall

The usefulness of the model is demonstrated in simulation of displacements of a retaining wall with the frost-susceptible backfill subjected to freezing. Figure 8 illustrates the initial and boundary conditions.

The commercially available system ABAQUS was used to generate the finite element grid and perform the calculations. The soil and the wall were divided into 750 elements. The elements used were 4-node plane-strain thermally coupled quadrilateral elements.

The vertical boundaries on both sides of the model are adiabatic, and the initial temperature is set to be uniform and equal to 3°C. At time $t = 0$ the external temperature drops down to -3°C, and it is kept at that level for the next 60 days.

The distribution of temperature and displacements after 60 days are illustrated in Fig. 9. The displacements are exaggerated by a factor of about 3.5. It is evident that the frost-susceptible soil heaved significantly. As the freezing front did not penetrate deep underneath the footing of the wall, the vertical displacement of the wall is small compared to the heave of the adjacent soil to the left of the wall footing. However, the wall tilted counter clockwise due to a considerable horizontal heave of the backfill immediately behind the wall. As the wall inhibits the horizontal displacement of the backfill, the upper surface of the fill "buckled out" as the moderate tilt of the wall could not accommodate the entire increase in the soil volume.

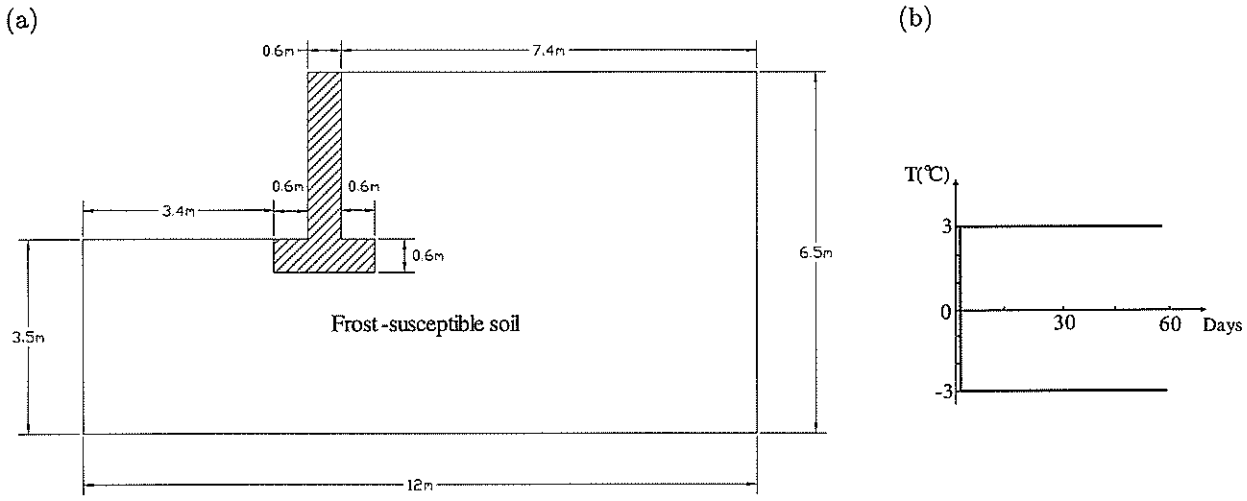

Fig. 8. Retaining wall: (a) geometry, and (b) thermal initial and boundary conditions

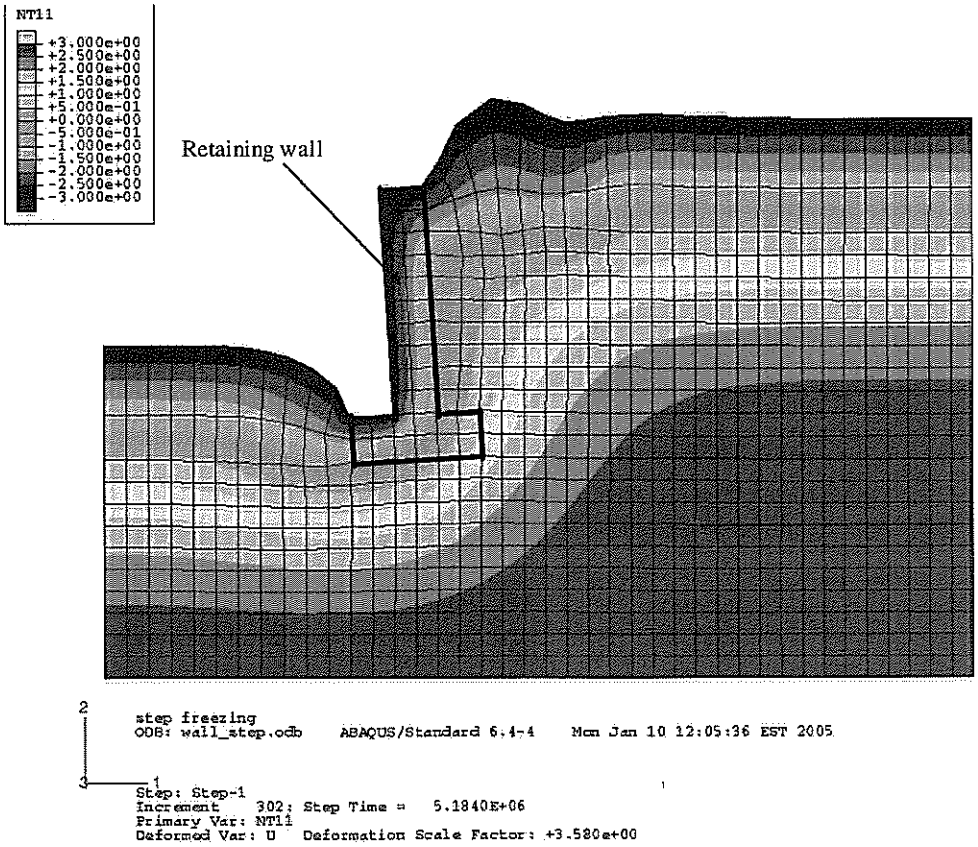

Fig. 9. Retaining wall displacement caused by frost heave

9. Influence of insulation on performance of retaining walls with frost-susceptible backfill

Since heaving requires the freezing front to move into the frost susceptible soil, it is expected that thermal insulation along the wall will inhibit the frost heave to some extent. To demonstrate the influence of the insulation on the performance of retaining walls, simulations were carried out of a freezing process for the retaining wall system illustrated in Fig. 10. First, a wall without insulation was simulated, and then simulations were performed for the walls with two different insulations.

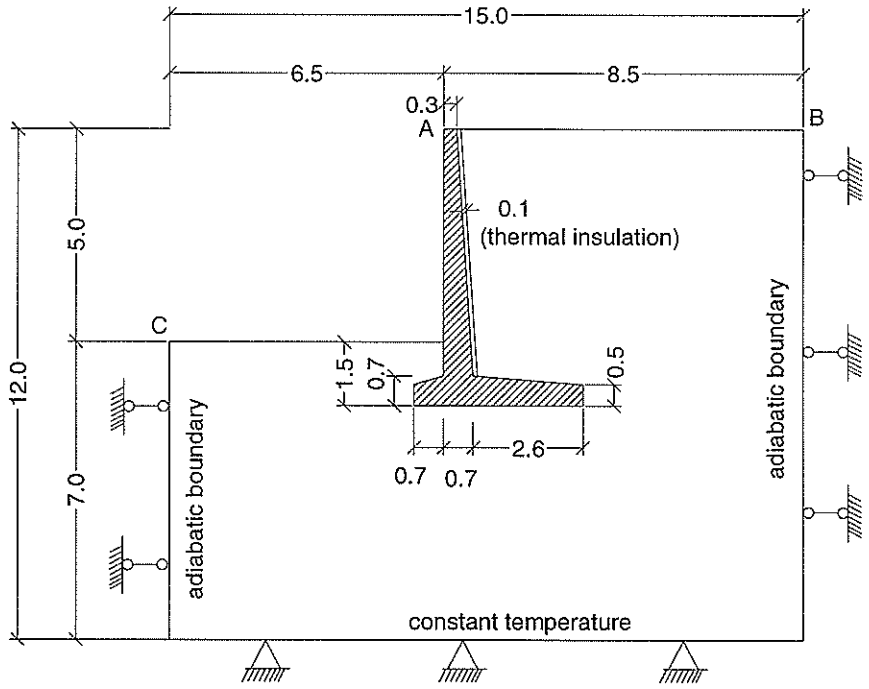

Fig. 10. Geometry of the retaining wall system with insulation (dimensions in meters)

The initial temperature distribution is shown in Fig. 11(a). The thermal boundary conditions are as follows: at time $t = 0$, the temperature along the external boundary suddenly drops from 1°C to −5°C, and it is kept at this level for 3 months (92 days), whereas the temperature at the base is kept steady at 3°C.

The finite element mesh is shown in Fig 11(b). The model is discretized using 4-node plane strain thermally coupled quadrilateral elements (ABAQUS type CPE4T). The total number of elements is 2950 and the total number of nodes is 3076. The soil material properties pertaining to heaving were adopted from the calibration based on the tests by Fukuda *et al.* [4] and presented earlier in the paper: $\dot{n}_m = 6.02 \cdot 10^{-5}\,\mathrm{s}^{-1}$ (or $5.2 \cdot 1/24\,\mathrm{h}$) at $g_T = 100°\mathrm{C/m}$, or $\dot{n}_m/g_T = 6.02 \cdot 10^{-7}\,\mathrm{m°C^{-1}s^{-1}}$, $T_m = -0.87°\mathrm{C}$, and $\zeta = 0.6\,\mathrm{MPa}$ (for details see Michalowski and Zhu [12]).

The elasticity parameters for the soil were taken as follows: Young's modulus equal to 11.2 MPa for unfrozen soil, temperature-dependent $E = 13.75|T|^{1.18}\,\mathrm{MPa}$ (T in °C) for frozen soil below −1°C (after Ladanyi and Shen [9]), and linear interpolation in the range 0 to −1°C; Poisson's ratio was taken as $\mu = 0.3$ for both the frozen and unfrozen soil. The remaining thermal parameters were: thermal conductivities: 1.95, 0.56, and $2.24\,\mathrm{Wm^{-1}K^{-1}}$ for the mineral phase, water, and ice, respectively; heat capacities: 900, 4180, and 2100 $\mathrm{Jkg^{-1}K^{-1}}$ for mineral, water, and ice, respectively; latent heat of fusion of water: $3.33 \cdot 10^5\,\mathrm{Jkg^{-1}K^{-1}}$. These were extracted from the literature [17, 21]. Parameter ξ that governs the anisotropy of the ice growth in Eq. (4) is difficult to assess, since no laboratory measurements are available for its evaluation. It is known, however, that the ice lenses grow predominantly in the direction of heat flow, and the value $\xi = 0.9$ was adopted.

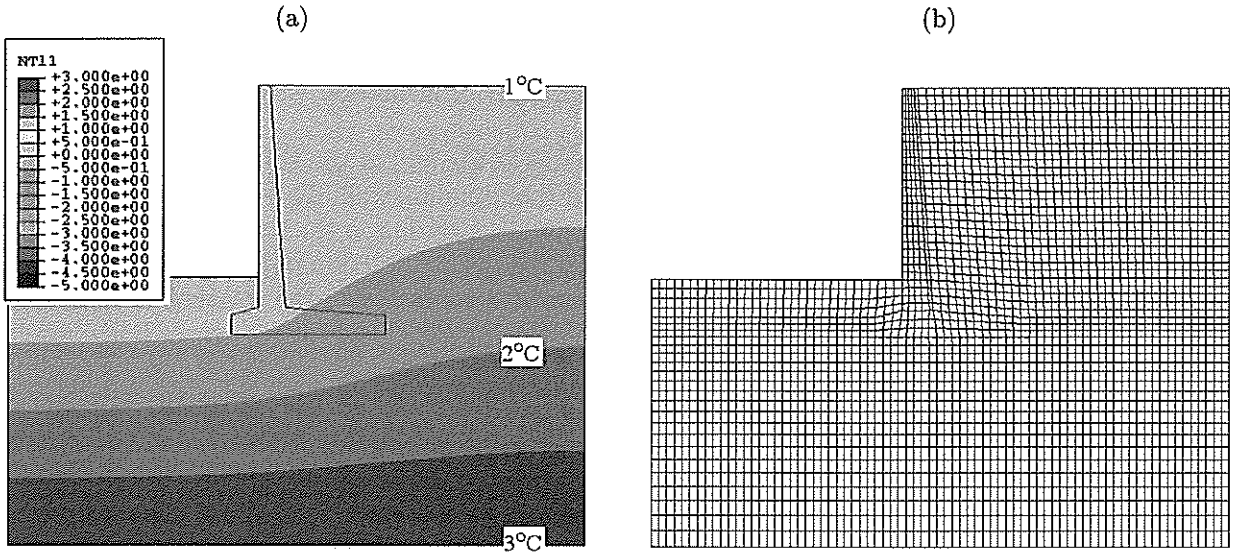

Fig. 11. (a) Initial temperature distribution, and (b) the finite element mesh

Table 1. Material properties of concrete and thermal insulation

	Density ρ (kg/m^3)	Mass heat capacity C (J/kg°C)	Thermal conductivity λ (W/m°C)	Young's modulus E (Pa)	Poisson's ratio μ
Concrete	2242	970	1.2	$2{\cdot}10^{10}$	0.38
Thermal insulation	50	2000	0.03 or 0.2	$1{\cdot}10^{7}$	0.3

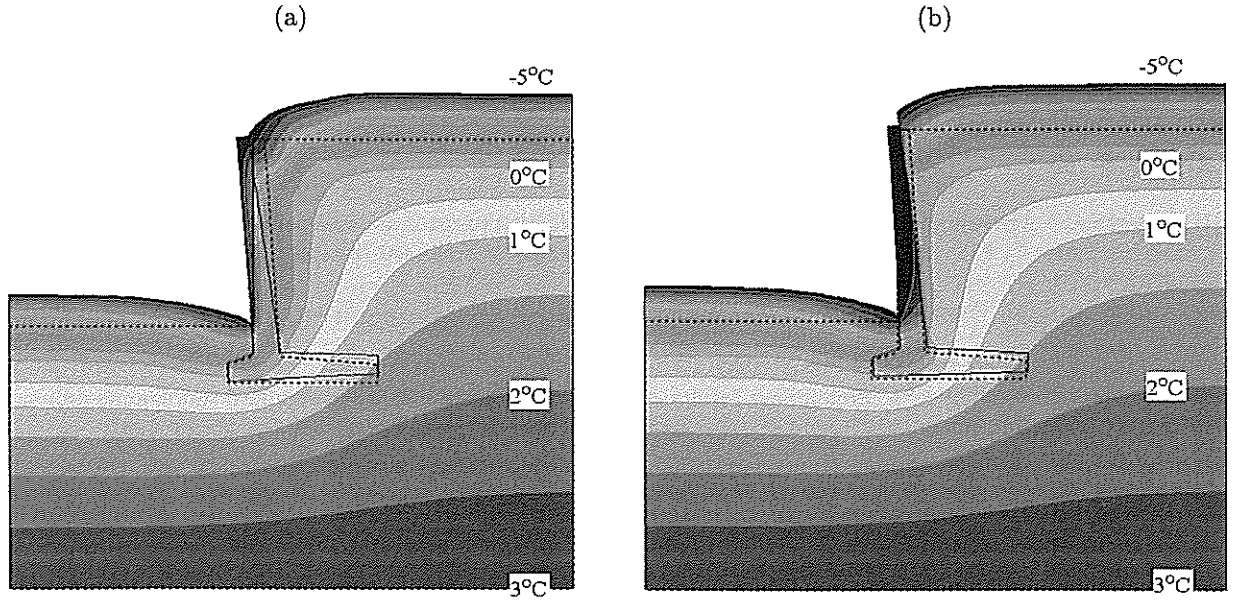

Fig. 12. Temperature distribution and deformation (exaggerated 2×) for: (a) the case with no insulation, and (b) with insulation $\lambda = 0.03\,\mathrm{W/m^\circ C}$

The material properties of the concrete wall and the thermal insulation are listed in Table 1. Three cases are considered to study the effect of the thermal insulation: (a) no thermal insulation behind the wall, (b) a 0.1 m thick layer of insulation on the backfill side of the wall, with heat conductivity of $\lambda = 0.2\,\mathrm{W/m^\circ C}$, and (c) a 0.1 m thick layer of insulation with a heat conductivity of $\lambda = 0.03\,\mathrm{W/m^\circ C}$.

The temperature distribution in the wall and the soil at the end of the third month is shown in Fig. 12(a) for the case of no thermal insulation behind the retaining wall. Also shown in the figure is the deformation. The contours relate to the temperature distribution in the soil. The displacements are exaggerated by a factor of 2. As the frost heave occurs in the direction of the heat flow, vertical displacements are considerable along the horizontal surfaces subjected to the freezing temperature. Along the wall, however, the isotherms are oriented vertically, thus the heaving occurs horizontally. The retaining structure is an obstacle to heaving, and the wall tilts.

The simulated horizontal displacement at point A (the tip of the wall, Fig. 10) is 0.208 m. With the insulation of $\lambda = 0.20\,\mathrm{W/m^\circ C}$ the horizontal displacement at point A was reduced by almost 20%, and when a more effective insulation was used with $\lambda = 0.03\,\mathrm{W/m^\circ C}$, the horizontal displacement at the wall crown was reduced by 42%.

10. Final remarks

Although phenomenological in nature, the model presented has the characteristics necessary to simulate the physical process of frost heaving. The model was calibrated using ramped freezing tests. Subsequently, a step-freezing process was simulated to validate the model. The simulation resulted in a very close prediction of the experimental results. Application of the model to solving boundary value problems is straightforward, and the results obtained for freezing of a frost-susceptible backfill behind a retaining wall appear to be quite realistic. As the frost heave is associated with the penetration of the freezing front into the frost-susceptible soil, the heave can be prevented to some extent by thermally insulating the structure.

Acknowledgement

The research presented in this paper was supported by the U.S. Army Research Office, Grant No. DAAD19-03-1-0063. This support is greatly appreciated.

References

[1] G. Beskow. Soil freezing and frost heaving with special application to roads and railroads. The Swedish Geological Society, Series C, 375, 1935 (transl. J.O. Osberberg, published by Technical Institute, Northwestern University, 1974).

[2] D. Blanchard, M. Frémond. Soil frost heaving and thaw settlement. *4th Int. Symp. Ground Freezing, Sapporo*, 209–216, 1985.

[3] M. Frémond. Personal communication, 1987.

[4] M. Fukuda, H. Kim, Y. Kim. Preliminary results of frost heave experiments using standard test sample provided by TC8. *Proc. Int. Symp. on Ground Freezing and Frost Action in Soils, Luleå, Sweden*, 25–30. 1997.

[5] G.L. Guymon, T.V. Hromadka, R.L. Berg. Two-dimensional model of coupled heat and moisture transport in frost-heaving soils. *J. Energy Resources Technol.*, **106**: 336–343, 1984.

[6] J.T. Holden. Approximate solutions for Miller's theory of secondary heave. *4th Int. Conf. Permafrost, Fairbanks, Alaska*, 498–503, 1983.

[7] J.T. Holden, D. Piper, R.H. Jones. Some developments of a rigid-ice model of frost heave. *4th Int. Symp. Ground Freezing, Sapporo*, 93–99, 1985.

[8] J.M. Konrad, N.R. Morgenstern. A mechanistic theory of ice lens formation in fine-grained soils. *Canadian Geotech. J.*, **17**: 473–486, 1980.

[9] B. Ladanyi, M. Shen. Freezing pressure development on a buried chilled pipeline. *Proc. 2nd Int. Symp. Frost in Geotechnical Engineering, Anchorage, Alaska*, 23–33, 1993.

[10] R.L. Michalowski. A constitutive model for frost susceptible soils. In: G.N. Pande, S. Pietruszczak (eds.), *4th Int. Symp. Numerical Models in Geomechanics, Swansea*, 159–167, 1992.
[11] R.L. Michalowski. A constitutive model of saturated soils for frost heave simulations. *Cold Regions Sci. Technol.*, **22**: 47–63, 1993.
[12] R.L. Michalowski, M. Zhu. Frost heave modeling using porosity rate function. *Int. J. Num. Analyt. Meth. Geomech.*, **30**: 703–722, 2006.
[13] R.D. Miller. Frost heaving in non-colloidal soils. *Third Int. Conf. Permafrost, Edmonton, Alberta*, 707–713, 1978.
[14] K. O'Neill, R.D. Miller. Numerical solutions for a rigid ice model of secondary frost heave. *2nd Int. Symp. Ground Freezing, Trondheim*, 656–669, 1980.
[15] K. O'Neill, R.D. Miller. Exploration of a rigid ice model of frost heave. *Water Resources Research*, **21**: 281–296, 1985.
[16] M.J.M. Römkens, R.D. Miller. Migration of mineral particles in ice with a temperature gradient. *J. Coll. Interf. Sci.*, **42**: 103–111, 1973.
[17] A.P.S. Selvadurai, J. Hu, I. Konu. Computational modeling of frost heave induced soil-pipeline interaction: I. Modeling of frost heave. *Cold Regions Sci. Technol.*, **29**: 215–228, 1999.
[18] M. Shen, B. Ladanyi. Modelling of coupled heat, moisture and stress field in freezing soil. *Cold Regions Sci. Technol.*, **14**: 237–246, 1987.
[19] S. Taber. Frost heaving. *J. Geology*, **37**: 428–461, 1929.
[20] S. Taber. The mechanics of frost heaving. *J. Geology*, **38**: 303–317, 1930.
[21] P.J. Williams, M.W. Smith. *The Frozen Earth, Fundamentals of Geocryology*. Cambridge University Press, 1989.